Nuclear Instruments and Methods 196 (1982) 361–379
North-Holland Publishing Company

PARTICLE IDENTIFICATION BY dE/dx SAMPLING IN HIGH PRESSURE DRIFT DETECTORS *

I. LEHRAUS, R. MATTHEWSON and W. TEJESSY
CERN, Geneva, Switzerland

Received 19 October 1981

Resolution limits of large dE/dx sampling detectors were studied systematically for pressures up to 5.5 atm in a variety of argon mixtures. The measurements were performed in a detector consisting of 64 pairs of 2×2 cm^2 proportional counters and a 50 cm drift space. Resolving power and linearity of response were measured for several quasi-simultaneous particles at higher pressures, extending the total detector depth to 41 m of NTP equivalent. The results show that resolution is consistently reduced with respect to predictions based on atmospheric pressure measurements for depths up to 7.7 m without drift (EPI detector). Influence of second-order effects and critical parameters affecting the resolution are analyzed with emphasis on compact detector design and relativistic rise region.

1. Introduction

The aim of this experiment was to determine the attainable resolution in dE/dx sampling detectors, using a set-up with dimensions close to the limits imposed by requirements for a compact colliding beam detector design. The present generation of already operational full-scale colliding beam devices which include particle identification by ionization measurements has been designed to work at moments less than the minimum of ionization, i.e. up to only about 2 GeV/c, reaching resolutions in dE/dx of, on the average, about 15% fwhm which is sufficient for this range.

On the other hand, the extension of the detector performance to higher momenta and therefore into the relativistic rise region demands, inevitably, overall resolutions better than about 8% fwhm. So far, only a very limited amount of direct experimental data has been forthcoming from this extreme range. If a limit of a "second generation" detector depth is set roughly at 2 m, it is clear that the pressure of the gas filling must be increased [2–4] in order to have an atomospheric pressure depth equivalent of at least 5 m. Unfortunately, the slope of the relativistic rise is markedly reduced at high pressures, cancelling the potential gain in resolution. The trade-off point should be investigated very carefully, bearing in mind problems related to scattering in thick-wall pressure vessels, mechanical rigidity and position precision, possible leaks, etc.

In a final design, any particular detector will be optimized for a given pressure. If technically possible, the sample size should be scaled as $1/p$, the practical limits being about 0.5–1 cm width, leading to several hundred samples in 2 m total depth. Note that at atmospheric pressure the optimum sample size is about 5 cm for argon. The signal wire diameter also scales as $1/p$. This optimization is clearly not feasible in a survey experiment where the main interest is in a comparison of performance of various gas mixtures within a wide range of working pressures. It is also very important to keep most of the "free" parameters (e.g. the reduced field strength E/p and therefore the drift velocity) approximately constant, if allowed for by operating conditions. Meaningful direct comparison of performance for various gas mixtures is then possible. A full-scale set-up allows detailed study and interpretation of second-order effects, which otherwise become obscured, and results are obtained without resorting to quite delicate extrapolations from reduced-scale prototype measurements.

2. Experimental set-up

2.1. The detector

The geometry of the detector was chosen with emphasis on the possible direct comparison with our previous measurements using the same sample number and size without drift, i.e., 64×4 cm [2] or 128×6 cm [5] at NTP. For a wider range of pressures, however, a reduced sample size is desirable so as to reduce the charge collection time across the sample. These considerations led to a design using 64 pairs of 2×2 cm^2 samples, giving a total active detector length of 2.56 m. The

* A shorter version of the first part of this paper was presented at the Int. Conf. on Experimentation at LEP, Uppsala, Sweden, 15-20 June 1980 [1].

0029-554X/82/0000–0000/$02.75

maximum working pressure was chosen to be 6 atm absolute with the possibility of operation below atmospheric pressure. Fig. 1 shows schematically the inner structure of the detector. The 64 pairs of $2 \times 2\,cm^2$ proportional counters with an additional pair at each edge are formed by parallel wires stretched with 1 cm spacing between Vetronite bars and crimped in copper pins. The signal wires (at ground potential) are of 25 μm diameter stainless steel (Stablohm 675), tensioned to 40 g. The ht grid and field wires are of 100 μm diameter stainless steel, tensioned to 100 g. The lower electrode (at a negative potential of a few kilovolts) is made of polished light alloy plate which is fixed together with the Vetronite wire supports to a rigid light alloy welded frame. A gating grid with identical spacing is stretched 0.5 cm above the ht grid. The field wires are connected to the lower electrode. Separated connections to all odd and all even wires of each of two grids allow for several potential distributions to be applied so as to vary the transparency of the grid system and to gate on/off the gas amplification. In the "open" state the inner grid is connected to the lower electrode and field wires; the outer grid has higher negative potential. The data acquisition electronics was designed to have an input

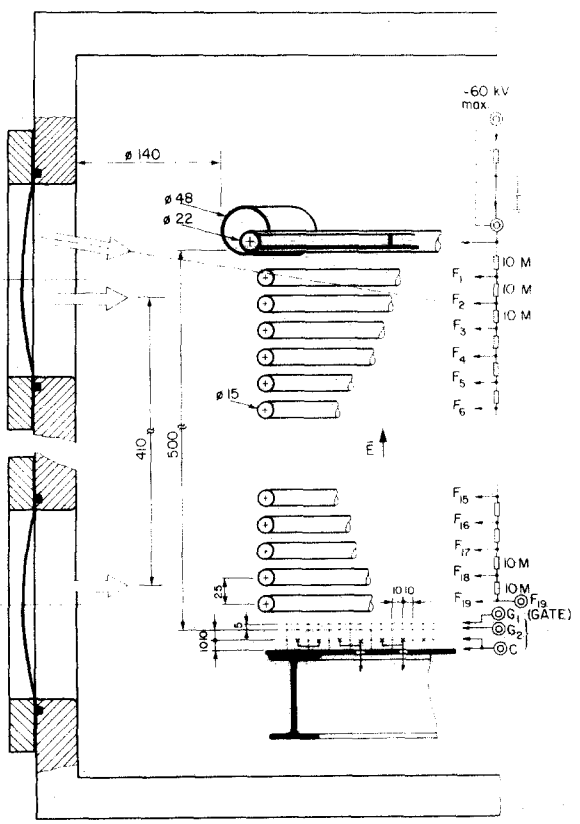

Fig. 1. Layout of the electrode structure.

sensitivity such that the gas amplification factor could be kept at 3×10^3 at NTP to assure linear ionization response.

For a most probable energy loss of about 1.5 keV/cm in argon (minimum ionization), 230 electrons are produced in a 4 cm sample giving typically 7×10^5 electrons in the avalanche. (The ADC saturation limit corresponds to less than 2×10^6 electrons.)

The product of the dE/dx deposit within the 4 cm sample and the gas gain was kept constant when varying the operating pressure, so that the gas gain was changing from 6×10^3 to 5×10^2 between 0.5 and 5 atm (amplifier and conversion gain were fixed).

The uniform electric field in the 50 cm of drift space is formed by a cage structure of 19 tubular stainless steel frames fixed with 2.5 cm interaxial spacing in five perpendicular Vetronite support frames. The tube diameter is 15 mm, the surface is polished and the corners of the frame are rounded with 3 cm radius. The beam entry and exit short frame sections have inserts of stainless steel tubes of only 0.2 mm wall thickness to reduce the amount of matter in the particle path. The drift space is closed by a polished stainless steel ht electrode (max. potential −60 kV) with a stainless steel tube of 22 mm diameter fixed around the edge to avoid corona. Two of the insulating frame supports contain the ht distribution chain of resistors of 10 MΩ per stage, encapsulated in Araldite. Polished "elbows" of 48 mm diameter stainless steel tubes are fixed to the electrode corners to reduce the critical field gradient. The electrode system was showing no discharge problems at full ht. The "short" dimension of the frames is 29 cm between the tube axes. From the 25.5 cm of the signal wire length, the middle part of ~15 cm length shows response uniform to within a few percent.

The measured electrostatic field maps for our grid configuration are shown in fig. 2. The drift field is 800 V/cm, the lower electrode is at 2 kV and the signal wires are grounded. Starting from the left, the first distribution corresponds to "open" state with maximum transmission through the grid structure. In the second field map the first grid is 900 V lower (if we assume the field gradient orientation from high in the drift region into a pit around the signal wire) with respect to the open state potential of 2.4 kV. In the third field map the first grid is put 500 V below the original potential of 2.4 kV and the second symmetrically higher by 500 V from the original 2.0 kV. In both cases the potential barrier created in the grid region seems to be partially transparent. In the next two field maps the ±500 V bias was applied symmetrically in a zig-zag pattern in both available combinations. The fourth distribution seems to be the most efficient for gating applications. In any case, a certain amount of charge will leak through. Also, the gas amplification factor will be strongly affected, as could be seen from the field modifications in the signal

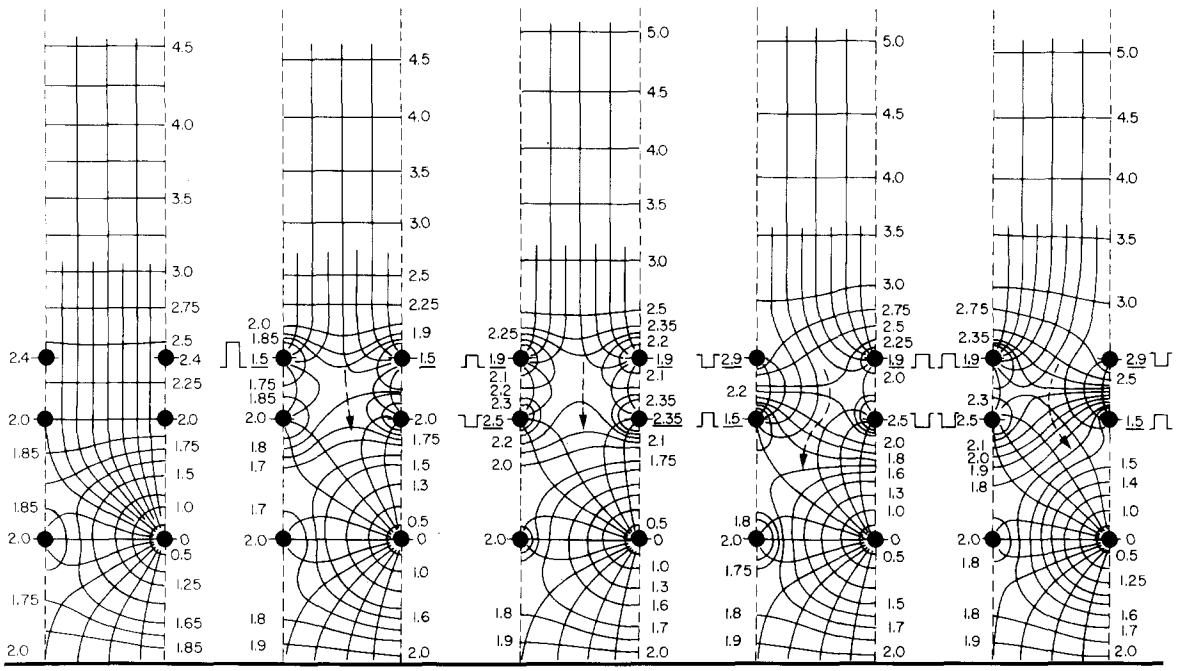

Fig. 2. Electrostatic field map for various combinations of the gating grid potentials.

wire region. Perfect balancing of the influence of two gating pulses of opposite polarity would be essential if pick-up by the amplifiers due to switching spikes is to be avoided. Fig. 3 shows, in the top part, the analogue signals from the wires, together with the switching spikes during the beam spill. The "open" gate pulse (corresponding to the second field map from fig. 2) was 800 V in amplitude and 90 ms long with rise and fall time constants of 500 μs. The lower trace is a trigger signal from the beam scintillation counter telescope. In the lower part of fig. 3 the gate was opened during the spill. The resulting spike has driven the signal amplifiers deeply into saturation for almost 20 ms. This is obviously the most unfavourable case and the symmetrical gating using balanced pulses will be much better, but all related problems are not yet solved.

The complete detector assembly as described above is suspended on insulators from a 5 cm thick steel lid which is bolted with O-ring seal to a rectangular shaped steel pressure vessel, so that the drift is taking place in the horizontal direction. The inner surfaces of the vessel are painted with an Araldite based vacuum paint. The minimum distance of the upper ht electrode from the vessel walls is 14 cm. The 60 kV connection is made via external RC filter through one of the big support insulators, sealed by O-ring. The other ht connections are made via separated vacuum-tight connectors. The signal wires are connected to a row of vacuum tight BNC coaxial connectors fixed in the lid.

Four 178 mm diameter 1 mm thick mylar windows

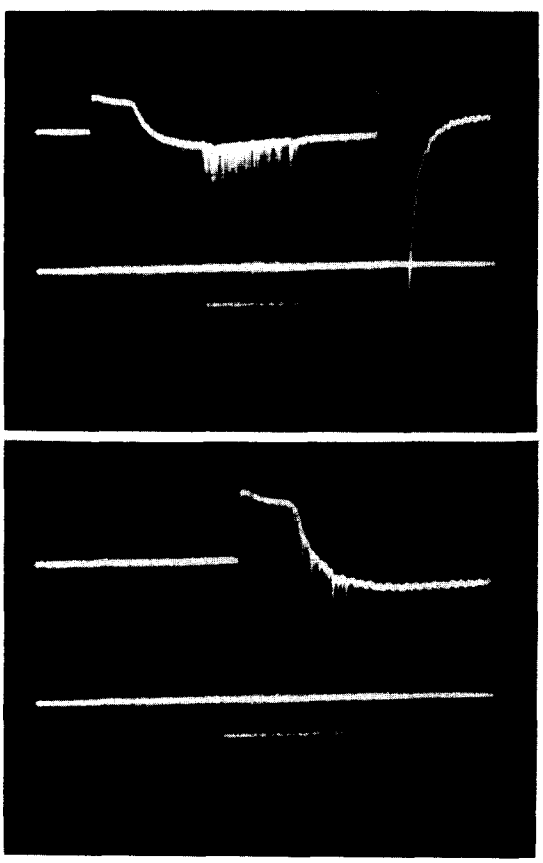

Fig. 3. Example of a gating action.

with Al foil sandwiched between the mylar sheets allow for alignment of the beam in "small drift", "full drift" and "diagonal" positions.

Two windows at 90° to the previous set were provided together with a reduced thickness in the upper electrode in the middle of the detector to enable a cursory investigation of the longitudinal drift along the particle trajectory. Fig. 4 shows an example of this longitudinal drift for a single particle in Ar + 20% CO_2 at NTP measured by a digital wave recorder. The drift velocity was close to 1 cm/μs. The upper part displays the full 50 cm of drift path at 50 ns sampling rate. In the lower part of fig. 4 the sampling rate was 10 ns; one horizontal division corresponds to about 0.5 cm (500 ns) of drift. The signal wire amplifier rise and fall times were 10 ns, but the time response was degraded by the 50 cm long cables inside the pressurized box. On the average, only 5 clusters/cm could be distinguished. The influence of diffusion in the gas is difficult to evaluate.

For monitoring and calibration, a collimated ^{55}Fe source equipped with a remotely controlled shutter was attached at one edge of the signal wire plane. A separate pair of $2 \times 2\,cm^2$ proportional counters with attached collimated ^{90}Sr source was situated inside the lower electrode support frame.

The system was positioned on rails fixed on a heavy turntable, so that the translation and rotation around the vertical axis permitted the beam to pass through the required parts of the drift volume.

Investigation of the influence of a magnetic field on the charge collection and linearity of response were not possible in our relatively thick and large steel pressure vessel. The necessary measurements therefore had to be performed separately using a small test chamber placed between the superconducting coils of the 3.7 m bubble chamber BEBC at the beam entry window. A group of three independent proportional counters of 4×4, 2×2 and $1 \times 1\,cm^2$ section were exposed to a high energy negative pion beam and the most probable value of ionization was measured in fields up to 35 kG by pulse

Fig. 4. Longitudinal drift in 50 cm. Ar+20% CO_2; NTP.

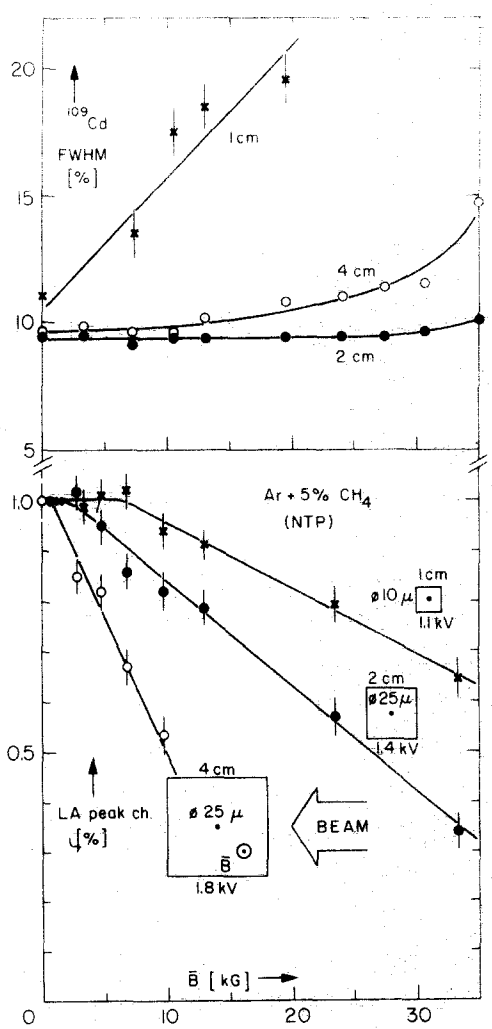

Fig. 5. Response of 1×1, 2×2 and $4 \times 4\,cm^2$ proportional cell in a magnetic field.

height analyser. At the same time the resolutions for ^{109}Cd 22 keV X-rays were determined. The signal wires, oriented parallel to the magnetic field direction, had diameters of 25 μm for the 4×4 and 2×2 cm^2 counters and 10 μm for the 1×1 cm^2 one. The gas filling was Ar + 5% CH_4 at NTP. The working conditions were optimized for maximum signal to noise ratio and linearity. The results are plotted in fig. 5, at the top for the width of the X-ray peak and at the bottom for the most probable ionization loss of the pions, normalized to zero field. As expected, the amplitude response in the latter case is immediately affected at low fields for 4×4 cm^2, the 2×2 cm^2 cell is significantly degraded from about 5 kG and the 1×1 cm^2 one seems to be operating correctly up to about 13 kG. For the X-ray resolution, by contrast, only the smallest cell shows significant degradation already at low fields. Therefore for a moderate field up to about 5 kG the 2×2 cm^2 cell seems to be the most reasonable choice.

2.2. Electronics

For a detailed study of the ionization amplitude response of the detector using gases having a wide range of drift velocities, it is preferable to use long time constants on the charge collection amplifier. This avoids an amplitude dependence upon drift velocity and small track angles, maintaining good measuring precision of the variations attributable to drift distance and gas characteristics. Also, measurements on quasi-simultaneous particle tracks are possible, since the limit imposed by double pulse resolution in fast electronics is avoided. Furthermore, a better signal to noise ratio is obtained, due to the longer integration of the ion current, which helps to increase resolution. Clearly, the particle rate must be limited accordingly.

Sixty four channels of the original EPI system [6] were modified to suit this study. The amplifiers were re-designed to have differentiating time constants of 20 μs, which gave a base-line to crest time of 6 μs when loaded with the input connecting cable and the detector. Under these conditions, the σ_{noise} was 6×10^3 electrons referred to the amplifier input which, when compared with the most probable signal value of 7×10^5 electrons, indicates a good signal to noise ratio. Resolution of the data acquisition electronics is 7×10^3 electrons and the ADC saturation limit 1.75×10^6 electrons.

Each pair of sample wires was connected to its integrating amplifier, track and hold and ramp comparison 8-bit ADC with shift register readout mounted directly on the detector. The ADC conversion time and readout into a local fast RAM buffer was about 450 μs. This was overlapped by a 500 μs re-triggerable veto gate, which defined the dead-time of the system and ensured that the data acquisition did not trigger again until the previous signals had well returned to the base-line.

For strictly parallel drift of tracks with respect to the signal wire plane, the common hold trigger and start of data acquisition were derived from a fast discriminator connected to a central sample pair. The error in measured amplitudes caused by errors and jitter in hold timing with respect to the pulse crest was about $\pm 0.5\%$ for 1 μs. The jitter was typically within ± 0.2 μs and the systematic part of this error was removed by individual sample corrections in the off-line data handling.

For diagonal tracks at fixed angle (fig. 1) the first hold trigger, derived from the edge cell, started an adjustable frequency clock, which provided consecutive equidistant triggers for the subsequent samples.

The string of 64 digitized pulse amplitudes corresponding to a given particle track was strobed first into the local fast RAM buffer which has a capacity for 16 tracks. The blocks of accumulated data were then transferred, between beam spills, via data link to a NORD-10 computer and written onto magnetic tape.

The arrival time of the signal from each particle was measured by a 20 ns resolution TDC as a difference between a beam tagging trigger and a stop pulse generated by the hold trigger discriminator and the result was also recorded on the tape. The drift velocity was determined over a 41 cm drift distance.

2.3. Layout of the beam tests

The detector was installed near the end of the S3 beam line in the E2 hall. Two ejections per SPS cycle were available, either of ~ 20–30 ms duration each, or fast spills of ~ 1 μs. The latter were used for the multitrack resolution studies. Systematic measurements of gas, pressure and drift dependence were performed at 15 GeV/c using a "natural" mixture of $\sim 10\%$ protons, $\sim 46\%$ pions and $\sim 44\%$ positrons; the muon contamination of the beam was negligible. The momentum bite was $\pm 0.25\%$ and the beam spot size was, at 15 GeV/c, ~ 4 cm fwhm in the horizontal (drift) plane and a little less in the vertical plane. The beam divergency was negligible inside the 2.56 m of active detecting volume; particle flux was kept, on the average, at ~ 10 per burst.

The detector was placed in front of the second of the beam tagging scintillation hodoscopes [7], so that the horizontal position of each particle was determined and registered with < 20 ns time resolution and within 0.5 cm in space. Two threshold Cherenkov counters identified positrons, pions and protons. An additional anti-halo large area scintillator with central hole for the beam was used for part of the run, covering most of the drift region exposed to the beam. Some of the electron showers generated near the end of the detector were eliminated in this way.

2.4. Gas system and choice of mixtures

The quality of the mostly metallic surfaces exposed to the gas, the Araldite coating of the Vetronite and good quality seals allowed for pumping down to almost 5×10^{-3} Torr. This corresponds, for a detector volume of some 1850 l, to a level of 2–5 ppm of O_2, improving with each consecutive pumping. A recirculation loop containing molecular sieve and "Oxisorb" purifier and membrane compressor was installed to be used for prolonged multiparticle resolution tests. The measured gas mixtures were filled into the detector in premixed form. Heating of the inlet tubes was necessary to speed up the stabilization of temperature during fast filling. The precision of the premixing was $\pm 0.5\%$ in volume.

The gas purity for the Ar + 5% CH_4 mixture used in long runs was 99.995% for Ar with an O_2 concentration < 5 ppm and 99.95% for CH_4 with $O_2 < 10$ ppm. For other measurements the Ar purity was 99.998% with $O_2 < 2$ ppm, the CO_2 purity was similar and the organic quenching agents were 99.95% pure with $O_2 < 10$ ppm.

The gas mixtures were selected so as to have close values of the drift velocity. The compilation of data from ref. 8 indicates that for a 1 kV/cm field strength the "common" point is near 4 cm/μs at NTP and, for the majority of the quenching agents, at $\sim 20\%$ concentration in argon. Mixtures of argon and 20% CH_4, C_2H_4, C_2H_6, C_3H_8 and CO_2 were used. For iC_4H_{10} the chosen concentration was 15%. 5% CH_4 was used for comparison with the extensive data available for this mixture at NTP. One should note here that argon and up to 9% CH_4 mixture is non-explosive (the explosive concentrations are on a few percent level for the other organic quenchers). Measurements were also performed for 5% C_3H_8, 50% C_2H_6 and for two more exotic mixtures with small amounts of xenon: Ar + 2% Xe + 15% CH_4 and Ar + 5% Xe + 15% C_2H_6. In order to improve the uncomfortably low drift velocity of CO_2, a mixture of Ar + 10% CO_2 + 10% C_2H_6 was used for some tests.

2.5. Data processing

Input of the particle data to the Nord-10 computer was through a common CAMAC direct memory access channel via independent real-time data streams for ionization values, drift time and tagging information, running under the SINTRAN III operating system. Separate logical records were written onto 1600 bpi magnetic tape from each of these data streams. Correlation of the streams was achieved via the absolute time, arbitration of resources was governed by semaphores. Furthermore, pressure and radioactive source information were periodically evaluated and summaries printed out.

The intrinsically low flux rate allowed parallel analysis of full data for on-line displaying, which included the build-up of the energy-loss distribution over all samples, the individual sample responses, the drift time and the truncated mean distribution, thus allowing quick and reliable optimization of running conditions and their maintenance throughout the runs.

The off-line analysis from data compressed onto high density tape (6250 bpi) was undertaken at the CERN computer centre. Due to the parallel triggering mode of operation no pattern recognition was needed, thereby reducing the cleaning to removing particles outside the beam region in the horizontal plane with the help of the tagging hodoscopes and to excluding the few obvious non-tracks and, for slow extraction, multiple tracks by simple non-biasing criteria. The variations in response of the different samples (originally typically 5%) were corrected for by using the most probable values of the individual sample dE/dx distributions predetermined from the same data. For the truncated mean distributions the mean vaues of the lowest 40% of ionization samples for each track were calculated to concord with the percentage used in EPI evaluations. Correlated tagging information was available for a priori mass determination.

2.6. Measurements

Each gas mixture was measured at 0.5, 1, 2 and 3–5 atm. First, the beam was aligned on the gating ht grids and the grid transparency optimized for a given drift field. This has been done via on-line display using the truncated mean distributions for tagged pions.

To illustrate this method an intermediate stage in the procedure is shown as an example in fig. 6 for Ar + 5% C_3H_8 at 2 atm. Three distinct regions defined by the beam hodoscope are plotted separately for particles passing through: (1) the signal wire region, (2) the inter-grid boundary region and (3) the adjacent drift region. The beam spread is sufficient to illuminate all of them without hitting the ht electrode. The higher ionization signals come, as expected, from the space nearest the signal wires, whilst the drift-region signals are attenuated due to transmission losses through the grids at these not yet optimized voltages. Nevertheless, the transmission efficienty is already at 94%. Not that due to the finite hodoscope resolution and the beam spread the "wires" plot also displays hits in the boundary region.

The aim of the exercise is now to adjust the grid potentials so as to merge the drift region peak with the direct peak from the wire region, reducing at the same time the prominance of the boundary peak and bringing it up towards the other two. In general this merging of the peaks can be achieved within two or three iterations, so that little data-taking time is lost.

On the average, ~ 5000 events were then ac-

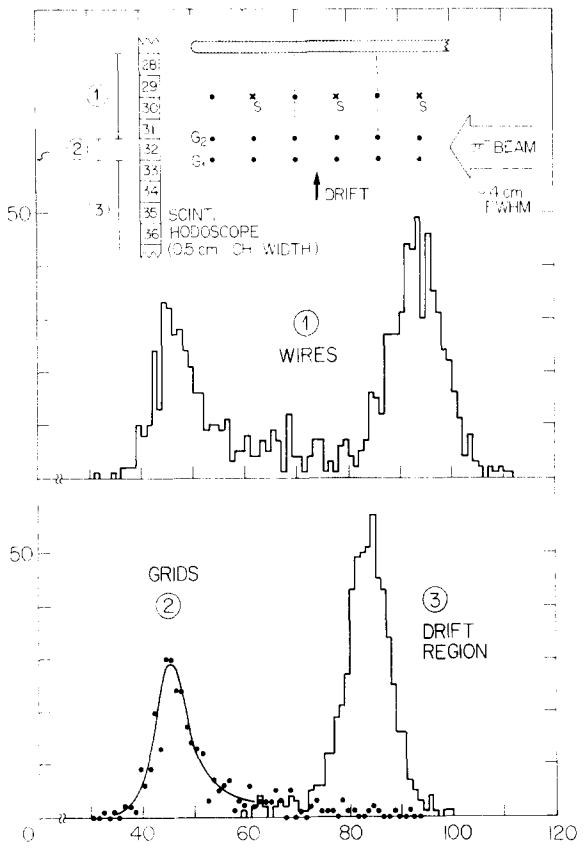

Fig. 6. Example of a grid transparency optimization procedure.

cumulated for each gas and pressure and in two parallel drift positions ("full drift", "small drift") spaced by 41 cm, as indicated by arrows in fig. 1. Control measurements were also performed along the diagonal of the detector at an angle of $\sim 10°$.

Generally, the applied drift fields in the drift region were in the range of 0.5–0.2 kV/cm · atm for 0.5–5 atm absolute pressure. In spite of the wide range of gas amplification factors for the various gas mixtures and sometimes conflicting requirements for the three correlated potentials the grid attenuation, measured via the ionization peak ratio between "wires" and "small" drift, was always well below 10%.

The cosmic ray background producing ~ 1–2 hits per spill was mostly vertical, influencing as a big signal only a few samples and thereby having little effect on the truncated mean. Most showers generated by electrons inside the detector were eliminated by the applied cuts. The beam was practically without halo. Protection against ejection spikes was provided by combined data acquisition veto and dead time defining gate. The data accumulation time was typically ~ 1 h for a given pressure and drift position. After temperature stabilization, the gas pressure was constant to within a few millibars at 5 atm.

3. Results

3.1. Resolution and relativistic rise

Fig. 7 shows an example of results obtained at 5 atm for a mixture of Ar + 5% CH_4 at full drift (raw data). The distributions in the top part were produced by

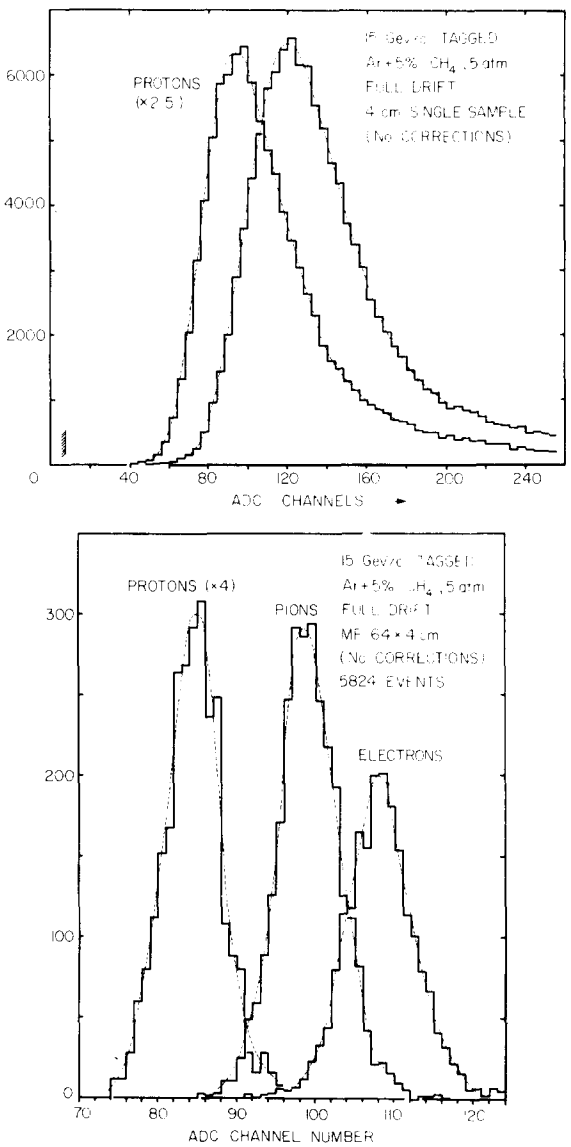

Fig. 7. Example of distributions obtained at 5 atm of Ar + 5% CH_4 in a tagged beam at 15 GeV/c (full drift). *Top*: 4 cm single sample distributions for protons and electrons. *Bottom*: Truncated mean of 64 × 4 cm samples for protons, pions and electrons. Resolution (uncorrected data): ~8% fwhm.

Table 1
Results for 15 GeV/c measurements on 64×4 samples (see text for details).

Gas mixture (% in Ar)	Pressure (atm)	E/p (kV/cm.atm)	v_d (cm/μs)	Atten. (% in 41 cm)	π's. LA	fwhm % (40%)	e/p (40%)	D/σ e/π	π/p
5 CH_4	0.5	0.36	2.60	0	86	14.0	1.509	2.96	4.84
	1.0	0.28	2.88	0	70	12.0	1.443	2.81	5.05
	2.0	0.19	3.46	0.5	61	10.0	1.367	2.87	5.18
	4.0 [a]	0.14	3.76	0.7	49	8.1	–	–	–
	5.0	0.11	3.97	0.6	45	7.6	1.287	2.75	5.62
	5.5	0.11	–	–	–	–	1.283	–	–
20 CH_4	0.5	0.54	6.14	0	84	17	1.488	1.97	4.08
	1.0	0.27	6.86	0	68	11.7	1.409	2.68	5.00
	2.0	0.28	6.81	0	59	9.3	1.341	2.71	5.28
	5.0	0.13	6.25	0.7	46	8.0	1.267	2.29	5.18
	5.5	0.19	–	–	–	–	1.267	–	–
2 Xe+15 CH_4	0.5	0.27	5.73	0	89	15.1	1.522	2.62	4.74
	1.0	0.27	5.68	0	68	12.0	1.420	2.67	4.98
	2.0	0.30	–	0	60	10.0	1.376	2.85	5.38
	3.3	0.23	5.78	1.7	52	8.1	1.314	2.87	5.71
	5.0	0.19	–	–	–	–	1.302	–	–
20 C_2H_4	1.0	0.27	4.44	0	70	12.0	1.405	2.53	4.90
	2.0	0.28	4.48	1.7	59	9.6	1.333	2.52	5.19
	4.0	0.16	3.58	3.7	50	8.6	1.281	2.31	4.89
	5.0	0.15	3.40	6.0	–	–	–	–	–
20 C_2H_6	0.5	0.28	5.23	0	75	14.0	1.443	2.24	4.94
	1.0	0.37	4.65	0	64	11.3	1.392	2.66	5.16
	2.0	0.39	4.67	0.6	55	9.0	1.315	2.79	5.14
	5.0	0.17	4.28	6.6	43	7.5	1.250	2.35	5.13
	5.5	0.12	–	–	–	–	1.250	–	–
50 C_2H_6	0.5	0.54	5.01	2.0	77	13.8	1.345	1.59	3.98
	1.0	0.57	5.00	9.8	57	10.4	1.285	1.84	4.35
	2.0	0.38	4.71	13.1	49	9.6	1.231	1.68	3.76
	4.0	0.24	4.01	47.9	40	8.3	1.193	1.60	3.48
5 Xe+15 C_2H_6	1.0	0.27	3.97	0	74	12.0	1.418	2.55	5.01
	2.25	0.28	4.03	3.6	60	9.9	1.339	2.80	4.87
5 C_3H_8	0.5	0.16	3.30	0	85	14.5	1.500	2.53	4.86
	1.0	0.28	3.36	0	70	11.9	1.427	2.73	5.05
	2.0	0.29	3.36	2.5	59	9.7	1.353	2.82	5.27
	4.0	0.18	3.43	3.8	50	7.7	1.298	2.76	5.73
20 C_3H_8	0.5	0.56	4.41	0	77	14.0	1.442	2.22	4.62
	1.0	0.27	3.88	5.1	63	10.1	1.355	2.52	5.20
	2.0	0.49	4.32	10.9	54	9.2	1.300	2.45	4.87
	4.5	0.24	3.69	24.6	43	7.5	1.240	2.37	4.70
15 iC_4H_{10}	0.5	0.44	5.10	0	77	15.5	1.437	2.16	3.94
	1.0	0.27	3.74	1.0	62	10.5	1.356	2.51	5.02
	2.0	0.28	3.81	2.8	51	8.4	1.302	2.64	5.40
	3.6	0.24	3.46	9.5	44	7.1	1.248	2.43	5.42
	5.0	0.17	3.40	–	–	–	1.244	–	–
20 CO_2	0.5	0.43	1.49	3.0	83	15.2	1.457	2.25	4.33
	1.0	0.27	0.90	5.2	67	10.9	1.410	2.87	5.29
	2.0	0.28	0.92	16.9	54	9.2	1.343	2.68	5.54
	3.5	0.24	0.78	35.8	48	8.3	1.284	2.41	5.23
	5.5	0.19	–	–	–	–	1.213	–	–
10 CO_2 + 10 C_2H_6	1.0	0.27	1.75	5.5	67	10.7	1.386	2.61	5.22
	2.0	0.24	1.53	16.0	56	9.4	1.331	2.81	5.03
	4.0	0.21	1.33	42.7	46	9.0	1.282	2.19	4.78

[a] Measured at 70 GeV/c.

directly plotting the 64 samples for each tagged track. In the lower part the truncated mean distributions for protons, pions and electrons indicate the reduced relativistic rise at 5 atm pressure. The resolution for data not corrected for sample response differences was ~ 8% fwhm.

In table 1 we summarize the final results from 15 GeV/c measurements on 64 × 4 cm samples. The first column contains the gas composition, the second the absolute operating pressure, followed by the reduced field strength, drift velocity and attenuation by attachment in the gas over the 41 cm drift difference expressed in percent. In the next column there is the single 4 cm sample Landau dE/dx distribution width in percent fwhm for pions, followed by final resolution of mean of 40% smallest values from 64 samples, also for pions. Next column shows the relativistic rise in terms of the ratio of truncated mean peaks of electron and proton distributions. The last two columns contain the resolving power for e/π and π/p expressed as the ratio of distance between the tagged peaks of truncated distributions for 64 samples to the standard deviation of the distribution for pions. The errors in the resolution, relativistic rise and in the resolving power are essentially given by the precision of determination of the peak value of a given dE/dx distribution, which, considering our adequate statistics, was rather pessimistically taken to be ±0.5 to ± 1.0%.

The resolving power D/σ is plotted in fig. 8 as a function of pressure. The top part of the plot shows π/p separation and bottom part the e/π separation. This plot is valid for 15 GeV/c; the resolving power will generally be better at lower and worse at higher particle momenta. Clearly, for dE/dx measurements there seems to be no "magic" gas which is considerably better than all others. The general tendency indicates that, with the exception of low percentages of CH_4 and C_3H_8, the gain by increased pressure becomes marginal already above 2 atm for π/p identification. Note that the e/π identification does not surpass the 3σ level and is slowly degrading for pressures above 2 atm. A low percentage of CH_4 or C_3H_8 looks more efficient here also. The

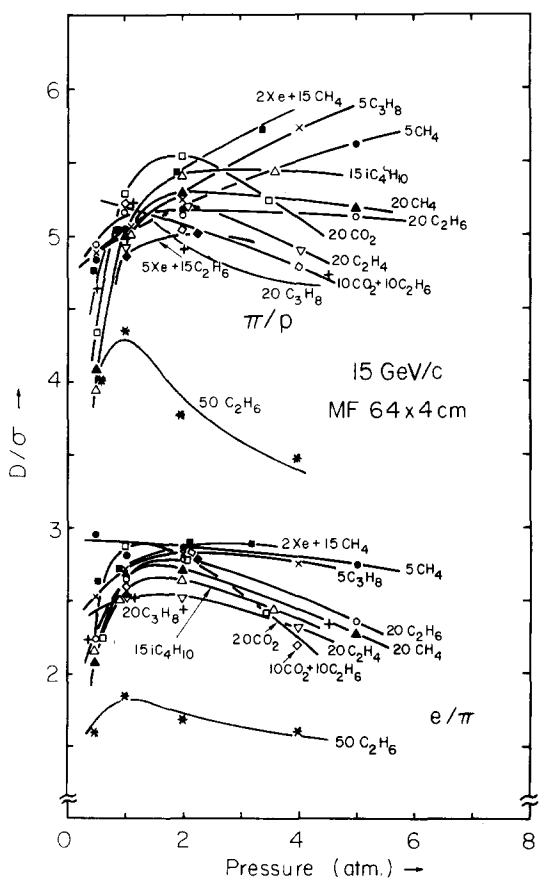

Fig. 8. Pressure dependence of resolving power D/σ for various gas mixtures at 15 GeV/c. Truncated mean of 64×4 cm samples. *Top*: π/p separation. *Bottom*: e/π separation.

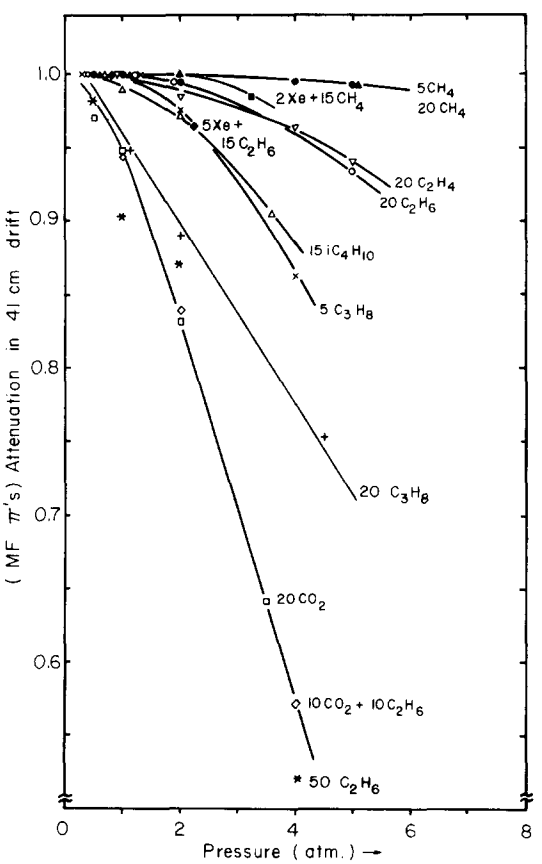

Fig. 9. Attenuation of the signal in 41 cm of drift as a function of pressure for various gas mixtures.

Table 2
Summary of relativistic rise measurements.

GeV/c	Particle	$\beta\gamma$	I/I_0			
			0.5	1.0	2.0	5.0 (atm)
5	π	35.8		1.260		
	e	9785		1.600		
10	π	71.6		1.365		
	e	19569		1.610		
15	p	16.0	1.127	1.125	1.125	1.124
	π	107.5	1.450	1.410	1.370	1.325
	e	29354	1.700	1.625	1.540	1.450
20	p	21.3		1.170		
	π	143.3		1.435		
	e	39139		1.610		
30	p	32.0		1.235		
	π	214.9		1.465		
	e	58708		1.600		
70	π	501.5		1.525		
140	π	1003		1.570		

influence of signal attenuation in the drift space was not taken into account.

The decay of signal due to electron attachment over 41 cm of drift distance as a function of pressure is plotted in fig. 9 as an average ratio of truncated means for tagged pions. With the exception of CO_2 and 50% C_2H_6 mixtures, most other gas mixtures are acceptable up to ~ 2 atm. The best results at higher pressures were obtained with 5% CH_4.

In principle, the electron attachment could be reduced by increasing E/p, but practical limitations caused by surface breakdown etc. will prevent any substantial improvements.

The relativistic rise measurements are summarized in table 2. The truncated mean ratios of protons, pions and electrons for Ar + 5% CH_4 were determined at 5, 10, 15, 20, 30, 70 and 140 GeV/c momenta. The errors are typically of the order of $\pm 0.5\%$. The corresponding plot is in fig. 10, which contains also data from ref. 5, together with results for 10 and 20% CH_4 from refs. 9, 10. The reduction of the relativistic rise slope and plateau values with increasing pressure is clearly marked. Part of the discrepancy visible at higher pressures could be explained by errors in the minimum ionization reference value and by different methods of measurements (single sample only in ref. 10).

In connection with theoretical predictions for probabilities of collisions with K, L and M-shell electrons [11], it is interesting to investigate the frequency of high-energy transfers producing overflows in the ADC. Fig. 11 shows an example of distributions of number of

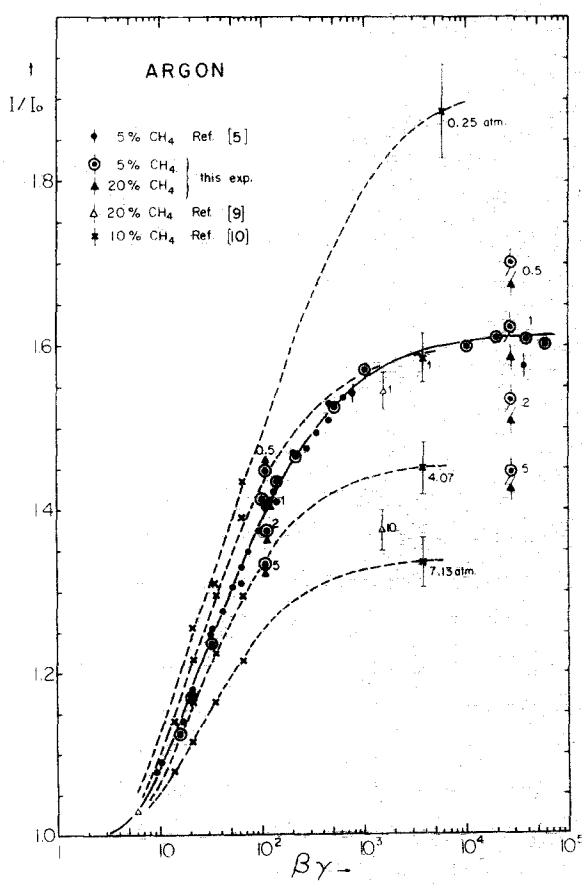

Fig. 10. Relativistic rise of ionization in Ar + CH_4 mixtures.

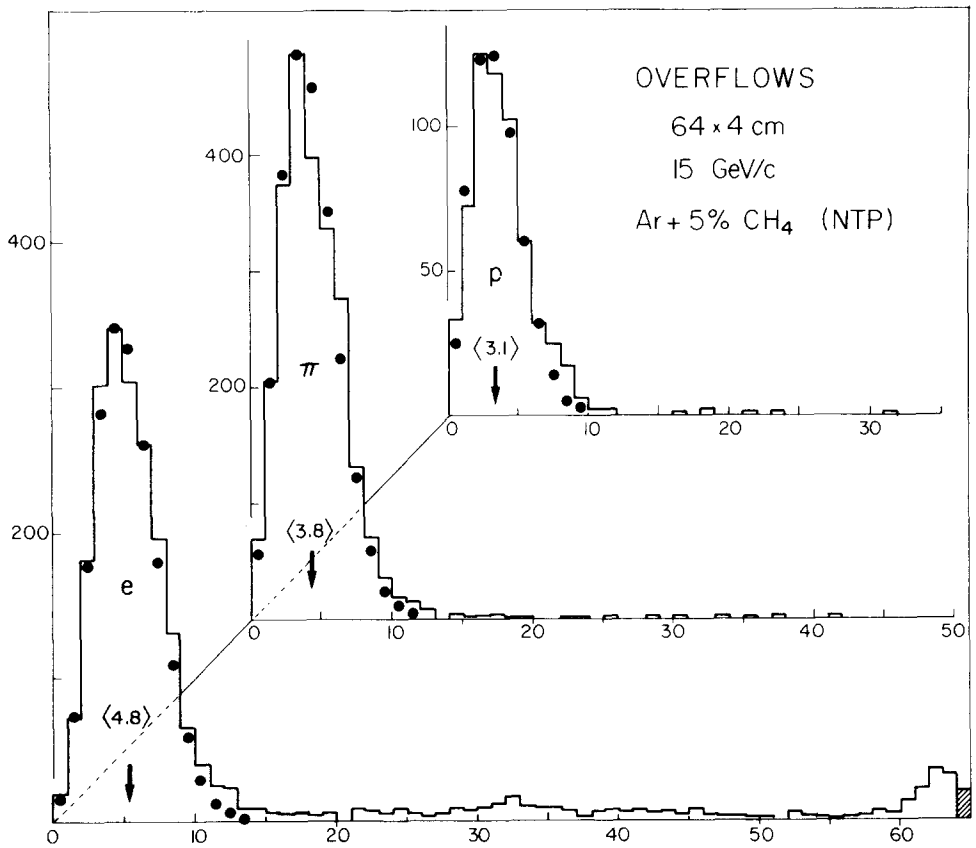

Fig. 11. Number of overflows in 64 samples for electrons, pions and protons.

overflows per electron, pion and proton at 15 GeV/c, in 64×4 cm samples (Ar + 5% CH_4, NTP). The corresponding single sample Landau peaks are at ADC channels 100, 88.5 and 69.5 respectively. The dots indicate Poisson distributions with mean values of 4.8, 3.8 and 3.1. The ratios of these values are 1.548 for e/p and 1.226 (π/p), which is to be compared to corresponding values of 1.443 and 1.258 obtained using the truncated

Table 3
Overflow data.

	Particle	0.5 (atm)	1.0 (atm)	3.3 (atm)
LA peak channel (8-bit ADC range)	e	83.0	89.0	96.5
	π	70.5	78.5	88.0
	p	55.0	63.5	73.5
Overflows in 64 samples (Poisson)	e	4.6	4.0	3.5
	π	3.5	3.2	3.0
	p	2.7	2.5	2.5
Overflow ratio	e/p	1.7	1.6	1.4
	π/p	1.3	1.3	1.2
(40%) peak ratio	e/p	1.522	1.420	1.314
	π/p	1.303	1.254	1.200
dE/dx(keV) of overflow	π	>2.3	>4.3	>13.1
Expected number of K-shell coll. in 64×4 cm		4	8–9	28

mean peaks. So even for these large energy transfers the relativistic rise is clearly present, but it is difficult to unfold the influence of changing shape of the Landau distributions and fixed position of the overflow limit or to overcome the problems caused by the widths of these distributions. Note that the tail from the bremsstrahlung in the electron distribution forms a general background without significant effect on the Poisson distribution.

In table 3 we list more complete overflow data from a mixture of Ar + 2% Xe + 15% CH_4 at 15 GeV/c, for 0.5, 1.0 and 3.3 atm. The single-sample Landau peak position is indicated for e, π and p within the 8 bit ADC dynamic range. The mean of the Poisson distribution fitting each individual overflow distribution and the ratios of the means from these fits are shown and compared to the corresponding truncated mean ratios. For e/p they are systematically higher, as can be seen, while the π/p ratios seem to be in good agreement. The energy loss at the overflow channel is equivalent to more than 2.3, 4.3 and 13.1 keV loss for 0.5, 1.0 and 3.3 atm respectively. The expected number of primary K-shell collisions is appended.

3.2. Multitrack resolution

Linearity of response, space charge saturation and its influence on the reliability of the amplitude measurements as well as general effects of the asymmetry of the energy-loss distribution were investigated for summed signals from quasi-simultaneous particles. The measurements were made in the full drift position with negative pions at 70 GeV/c, using a gas mixture of Ar + 5% CH_4 at 1 and 4 atm. Up to ten particles per fast spill of $< 1\,\mu$s produced a beam spot of < 2 cm diameter, which was elongated horizontally by the drift velocity of 2.9 and 3.8 cm/μs at 1 and 4 atm, respectively, in the space–time reference frame.

Fig. 12 shows the truncated mean distribution for multiple simultaneous particles at 4 atm. Whilst the abscissa is continuous (above 20), the ordinate scale has been changed repeatedly to allow a clearer display of the differently populated peaks for single, double, triple and quadruple particles. The clear separation between the different multiplicities furthermore allows to present the experimental single sample dE/dx distributions for each of these separately, as is shown in fig. 13 for 1 and 4 atm. The areas under the curves are normalized to the single particle distributions. The corresponding peak positions, in terms of ADC channel number, and the widths in percent fwhm are listed in the top half of table 4 for 1–4 simultaneous particles together with the ratio of the peak position of the truncated mean of n particles to single particles, renormalized as described below. It should be underlined here that the overflow limit was sufficiently high to prevent any overflows from introducing themselves into the truncated mean of the lowest 40%.

The gas amplification for this set of data had been reduced to about 1.5×10^3 for 1 atm and 0.4×10^3 for

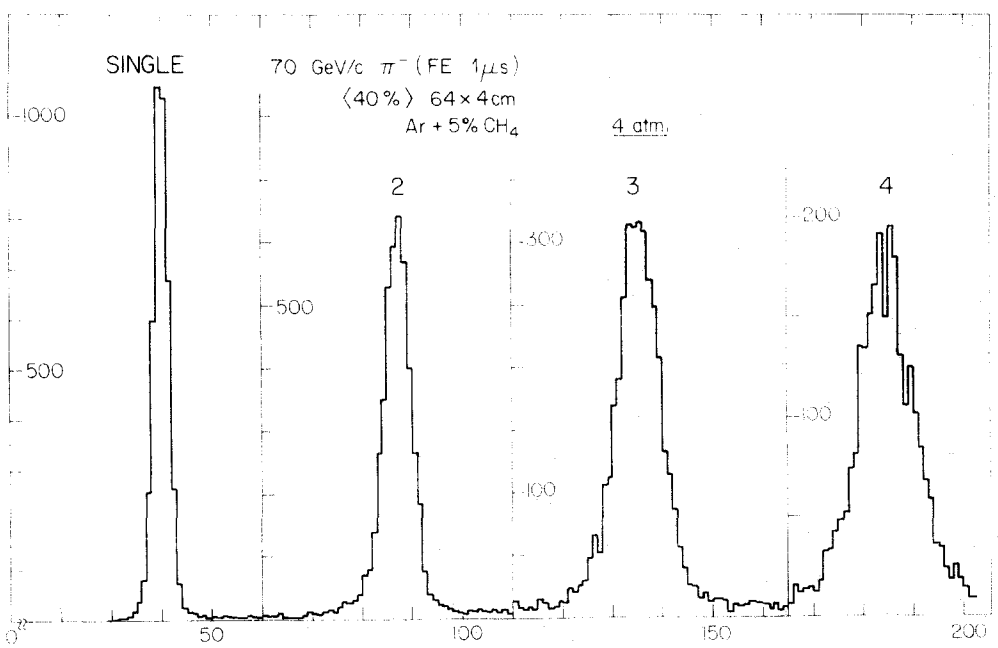

Fig. 12. Truncated mean distribution of 64×4 cm samples showing single, double, triple and quadruple particles. 70 GeV/c pions in Ar+5% CH_4, 4 atm.

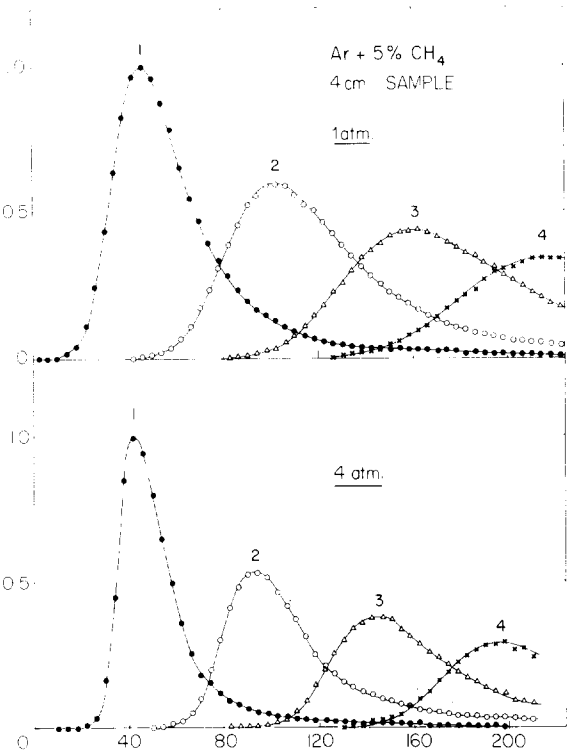

Fig. 13. Single 4 cm sample distributions for 1, 2, 3 and 4 particles in 1 and 4 atm of Ar+5% CH_4.

4 atm in order to shift the double particle peak into the optimum position within the ADC range. To further increase the range of multiplicities at both pressures the gas amplification factors were reduced by another factor of two leading to the results listed in the bottom half of the table for up to eight simultaneous particles. The shown ratio of multiple to single particle peak position for the truncated means has been renormalized to the centre of the particle range by choosing the 4 particle peak as reference and setting its ratio to 5, which gives approximately 1 for the single particle ratio.

Two interesting points stand out when regarding the figures and are corroborated by the listed data: the truncated mean peak position increases more rapidly than the multiplicity, reaching e.g. about 5 × the single particle value for a multiplicity of 4, and the composite dE/dx distributions do not emanate from the single particle distribution by simple appropriately renormalized multiplicative transformation of the form $x_i \rightarrow ax_i$, or, for that matter, although less clearly visible, by a linear transformation of the type $x_i \rightarrow ax_i + b$, due to more pronounced reduction of the width. It should be remarked that this non-linear behaviour with increasing ionization deposit renders correct maximum likelihood fitting difficult.

To look into these effects in more detail the single particle distributions, which due to the low amplification factors were well measured up to 5 times the peak values, were used as probability distribution references for extensive simulation of multiparticle results. It was found that the fake multiple particles reproduce exactly

Table 4
Peak positions and their fwhm for multiple particles

Number of particles	1 atm					4 atm					
	LA		(40%)			LA		(40%)			
	Peak	Fwhm	Peak	Fwhm	Ratio	Peak	Fwhm	Peak	Fwhm	Ratio	Fake
1	45	72	39.0	12.2	1.01	42	52	39.5	7.9	1.08	0.99
2	98	57	88.2	9.6	2.28	92	43	86.7	6.7	2.36	2.27
3	154	54	139.5	8.3	3.61	144	37	134.7	6.5	3.67	3.61
4	214	–	193.0	7.5	5	194	(32)	183.7	6.3	5	5
1			21.8	12.5	0.98			20.7	10.5	1.06	0.99
2			50.5	10.5	2.26			45.8	7.5	2.35	2.27
3			80.5	9.1	3.61			71.5	7.3	3.66	3.61
4			111.5	8.2	5			97.6	7.3	5	5
5			142.3	8.0	6.38			125.2	7.1	6.41	6.41
6			174.5	8.0	7.83			154.0	7.2	7.89	7.86
7			206.5	(7.7)	9.26			182.5	6.8	9.35	9.30
8			–	–	–			211.2	(6.3)	10.82	10.78
9			–	–	–			–	–	–	12.25
10			–	–	–			–	–	–	13.72

the dE/dx distributions found experimentally and that the peak position ratios for the truncated means coincide remarkably well, as shown in the column "Fake" of table 4, with the experimental data over the full range from 1 to 8 particles and for both of the regarded pressures. Thus, the found behaviour of multiple simultaneous particles can be fully explained as the addition of ionization from single particles following a typical Landau dE/dx distribution, and we may conclude that within the sensitivity limit of this method of about 1%, no anomalies in detector response due to clouds of migrating ions or saturation effects provoked by drift and arrival of the first particle to the vicinity of the signal wire are detectable.

It further follows that the described accentuated increase of the truncated mean peak position with increasing multiplicity is simply due to the effect of the narrowing of the asymmetric dE/dx distribution on the mean of its own lowest 40% of values. In fact while, for instance, the overall mean for 4 particles is 4 times the single particle mean, this value increases to 4.5 for a truncation cut at 80%, to 5.0 for 40% as already shown, and to 5.4 for lowest 20% of values taken. So the separation of peaks is enhanced for reduced truncation percentage, but unfortunately this gain is offset by greater statistical fluctuations, as can be seen in fig. 14.

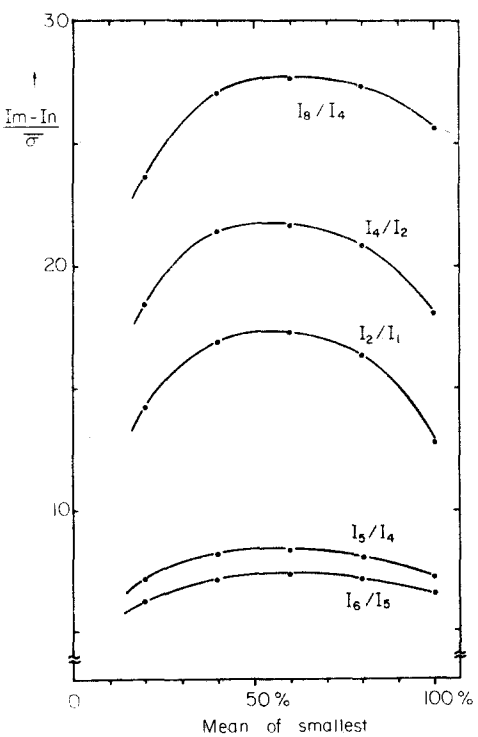

Fig. 14. Truncated mean response for multiple particles with the percentage taken for the truncation as a parameter, expressed in ratios of peak values for up to 8 particles.

which gives the resolving power between peaks of different multiplicities as a function of the truncation percentage extracted from the simulated data. As can be seen, the resolving power forms a broad plateau between 40 and 70% and the separation efficiency is not affected by the choice of truncation percentage in this region.

The change in asymmetry in the shape of the Landau distribution has been evaluated in table 5, again using the simulated data. The number of particles, the equivalent sample size, the peak position of the Landau distribution and the ratio of the most probable value to the overall mean are listed. When extrapolated to 1 cm sample equivalent, the data are consistent with the ratio of 0.60 obtained from most probable (42) and mean (70) number of primary electrons.

The results in the first part of table 4 are clean enough so we could use them to extend the resolution studies up to 41 m of total detector depth NTP equivalent, assuming the sample size to be a product of (thickness × pressure × number of particles).

Another method was used to analyze the detector performance with more precision. A matrix of scintillation counter hodoscopes with 0.5 cm channel width determined the horizontal and vertical positions of 2 particle hits within the 2 cm diameter beam spot. The drift time difference between the first and the second particle was measured by a TDC. Combining the position and drift time information, the real distance between any pair of particles was obtained. Fig. 15 shows the truncated mean of 64 × 4 cm samples for all pairs of "simultaneous" (summed-up signals) particles, both hitting the same vertical hodoscope strip, plotted against the particle distance Δx in cm. The pressure of the Ar + 5% CH_4 gas mixture was 4 atm, the beam spill was below 1 μs, the drift velocity was 3.76 cm/μs, the gas gain was about 400, the E/p was 0.14 kV/cm · atm. If a perturbation of the response for the second particle was

Table 5
Change in asymmetry in the shape of the Landau distribution.

Number of particles	Sample size (cm · atm)N	LA peak value	Ratio LA/mean
1	4	45	0.72
2	8	98	0.78
3	12	154	0.82
4	16	214	0.86
5	20	274	0.88
6	24	333	0.89
7	28	394	0.90
8	32	457	0.91
9	36	521	0.92
10	40	581	0.93

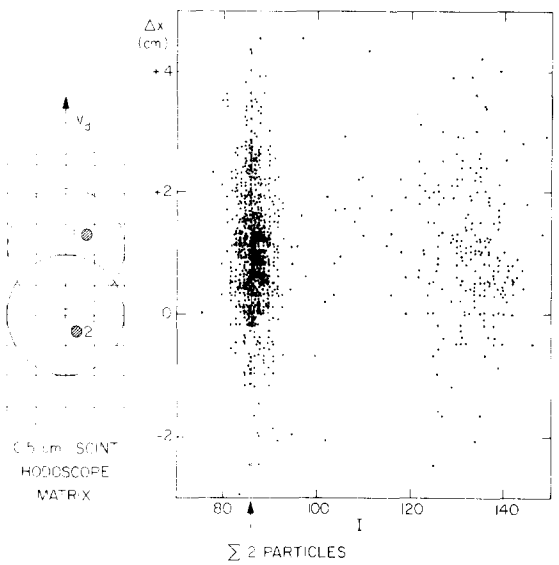

Fig. 15. Truncated mean for selected pairs of particles within the same 0.5 cm wide strip, plotted against their real distance during drift. Ar + 5% CH_4, 4 atm.

caused by space-charge and saturation from the first particle, one would expect the scatter plot in fig. 15 to show a tendency to decreased values of sum of two particles as a function of their distance. The scatter diagram looks perfectly symmetrical with respect to the mean value indicated by the straight line. In addition, there seems to be no difference for positive and negative Δx values, where negative Δx means cases when the second particle deposited its ionization loss in a "virgin" gas volume with no influence by the first ionizing track. The sensitivity of this method is of the order of one percent "non-linearity". There is no contamination of the double particle sample by accidental triple particles, since these clearly do not affect the double particle region. The fraction of truly simultaneous hits within the tagging resolution interval of 20 ns is negligible (these events will produce artificial coordinates in the Gray-coded horizontal hodoscope, leading to confused Δx information).

4. Conclusion

Fig. 6 shows the summarized data for resolution obtained in 64 × 4 cm samples in Ar + 5% CH_4 mixture as a function of pressure and number of simultaneous particles, expressed in terms of NTP equivalent of total detector depth of m · atm of argon. The results attained so far in prototypes or full-scale devices of this type are also plotted: TPC [9] CRISIS 1[12], ISIS 1[13], JADE [14], CLEO [15]. The numbers in brackets in the figure indicate the number of samples used for a given total detector depth.

As a curiosity, the single-sample detector [16] using a geometrical cut to remove the δ-ray influence is also included.

The dashed curve represents the expected performance for 64 samples, based on the results for 62 × 4 cm (EPI test modules [2]) and 64 × 6 cm (1/2 EPI). Full 128 sample EPI results [5] are also shown.

Clearly, there is a descrepancy between the predictions derived from the EPI results obtained under very favourable conditions at low flux for true single particles without background tracks and without drift, and our present data measured under more severe operating conditions (background and noise from the drift region). High pressure in itself cannot be the cause, because the resolution at 0.5 and 1 atm is already worse than the EPI atmospheric pressure data. The apparent discontinuity between the pressure dependence for single and multiple particles could be explained by better running conditions for multiple particles (fast ejection as for the EPI) combined with increasing influence of residual second-order effects which become more pronounced at higher total depths. This was verified for double particle 4 atm data from fig. 15: Very carefully applied supplementary selection criteria lead to a resolution of 6.3% fwhm, as compared to the original value of 6.7% from table 4. The additional data points measured in Ar + 20% C_3H_8 and Ar + 15% iC_4H_{10} show better performance, but it should be remembered that the gain in resolution is neutralized by reduced relativistic rise in those mixtures, as shown in figs. 8 and 9.

In the following paragraphs we give a complete as possible compilation of systematic second-order effects which affect the resolution. Some of them are practically undetectable in small-size prototypes of detectors. Obviously, it will be difficult to remove all of them; some could be attenuated by careful design or corrected for and some of them would have to be tolerated.

a) The momentum definition of our beam was more than adequate. This could be a problem in some colliding beam detectors (1–2% precision required).

b) Noise in the detector and electrical pick-up was in our case giving r.m.s. signal to noise ratio of 70:1, which may possibly be improved even in a larger detector set-up.

c) The non-uniformity of response along the signal wires was measured to be within ±2%, which will be difficult to realize for very long wires in presence of gravitational sag and electrostatic forces.

d) Residuals from uncorrected differences of response of individual wires within pairs of 2 × 2 cm^2 cells were estimated to be at ±2% level [20], comparable to the residual level of the off-line sample corrections. The mechanical precision, wire diameter uniformity and positioning are such that the original differences in

response are concentrated mostly in the amplifier input circuits.

e) Asymmetry of electrostatic field distribution within the samples caused by ht plate at one side and rather coarse grids at the other side of the signal wire are not important for charges drifting always from the same side and for low gas amplification factors.

f) Jitter in common hold trigger for data acquisition caused by diffusion, angle and deformation of tracks by non-uniformities in the drift field near the electrode structure was, in our case of relatively slow integration, responsible for less than $\pm 1\%$ of amplitude changes.

g) Background tracks, interactions and decays, ejection spikes etc. were mostly removed by veto and dead-time defining gates. The already small beam halo could be taken care of by a veto scintillation counter. This type of background was also suppressed by the truncated mean method which rejects big ionization fluctuations. Relatively low flux and dc coupled electronics avoid pile-up and baseline shifts. No difference has been found between first and second ejection when both the rate and spill length were different by more than a factor of two. A detectable shift occurred only at unvetoed flux of 60–70 particles per spill, whereas the normal running conditions were 10 particles or less.

h) Residuals from corrections of pressure and temperature variations were small. No detectable change appeared during roughly 1 h intervals required for accumulation of typically 5000 events. In the worst case the degradation of pulse heights due to outgassing was -3% per day and was easily monitored.

i) The cross-talk between adjacent samples caused by diffusion during drift is to some extent inevitable, but it was quite small in our case for 4 cm sample width compared to a typical value of diffusion of the order of 100 μm/cm of drift. This effect will spoil the resolution by "averaging" the adjacent samples.

j) The cross-talk caused by direct coupling of adjacent samples through partially transparent field barrier was measured using longitudinal drift. It was found to be about 0.3% of integral charge penetrating into the next sample, and no influence was detected in more distant samples.

k) To avoid saturation problems, the gas gain was kept sufficiently low (at 3×10^3 for NTP) to assure perfect linearity of response. Any saturation effects would superpose themselves on the true relativistic rise and resolution-erroneously reducing the slope of the former and the fwhm of the latter.

l) The positive induced charge in the adjacent samples causes a reduction of measured pulse amplitudes similar to the baseline shift influence. This is the most critical problem if a rather difficult compromise between requirements for good decoupling of all ht grids and for gating operation conditions is to be found. In our case the decoupling was sufficient to limit the absolute broadening of the resolution to about 0.7%. A matrix of necessary corrections could be determined and used off-line, but it would be difficult to correct inclined or curved tracks in presence of background.

m) The influence of space-charge (positive ions) in the drift region was checked using multiple particles and was already discussed in detail. Deformation of tracks, due to diffusion, was fully accomodated by the long time-constants of the current integrator.

n) The space-charge in the avalanche near the signal wires and possible saturation was checked by comparing the response of the first particle in a given spill to all others. The result was showing reductions of the order of $(1 \pm 0.2)\%$ for the peak position of the rest of the spill; the resolution was not affected. This effect was confirmed in some cases by a slightly higher peak position (by about 0.5%) for full drift with respect to the small drift position, where the space-charge influence was reduced by diffusion occurring during longer drift

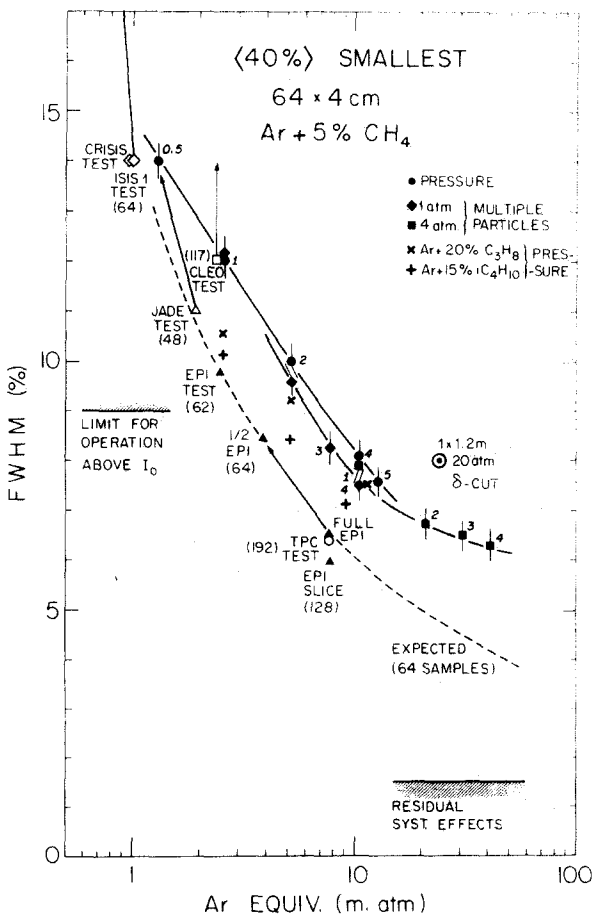

Fig. 16. Present "state of the art" in the resolution range required for relativistic rise applications, as a function of total detection depth in cm·atm of argon.

distance. These problems were already extensively treated for multiwire proportional chambers [17].

The influence of none of the individual efffects mentioned above is by itself strong enough to be responsible for the observed broadening of the resolution. It is, of course, to be expected that a combination of these essentially second-order effects might appear on a sufficiently high level to be of influence. In our case, the most important contribution, estimated to account for $\sim 1/3$ of the "missing resolution", seems to stem from positive induced charges.

Without trying to find a complete and exact explanation of the complex mechanism involved, we offer the following "rule of thumb" for realistic estimation of resolution of detectors of similar size: the experimental resolution of a detector will be roughly equal to the previously predicted resolution of a device having half its sample size. This includes a safety margin that is necessary for compensation of loss of samples due to background and some crossing tracks in a full-size detector. In that case, the detector design parameters could be determined from the correspondingly updated graph in ref. 2 or using modified semi-empirical formulas proposed in refs. 3 and 4.

In fig. 17 the three above mentioned design guides are compared. The "original" resolutions of 5 and 10% fwhm are shown as a function of number of samples of a given thickness as a parameter. This resolution must be obtained for relativistic rise region applications. The 5% limit will be very difficult to reach because of the influence of the second-order effects discussed in the previous paragraphs. Curves marked 1, 2 and 3 are from refs. 2, 3 and 4 respectively. For sample sizes varying from 2 to 16 cm · atm of argon, the differences in predicted resolution are marginal. The curves 1 and 3 are slowly rising with increasing number of smaller samples. This reflects the effect of faster broadening of resolution of smaller samples (worse signal/noise ratio), which is not fully compensated by gain in number. Our present results for 1, 2 and 4 particles at 4 atm are also indicated, together with the EPI data.

In table 6 we present the results of joining subsequent tracks from the experimental clean single particle distributions (1 and 4 atm, Ar + 5% CH_4) in order to compare gains in resolution which could be obtained by doubling the number of 4 cm samples. The net gain in resolution corresponding to an increase from 64 to 128 and 256 samples is each time about 20%. The number in brackets indicate resolutions expected from extrapolated atmospheric pressure data without drift.

When the total depth is kept constant, i.e. when the sample size is halved and the number doubled, the corresponding gain in resolution is only about 10%.

The best performances were obtained for gas mixtures containing relatively small percentage of CH_4 or C_3H_8. Methane showed smaller attenuation of signal during drift. The improvement of resolving power with pressure was rather marginal above 2 atm.

The gas purity was found to be not too critical for O_2 concentrations up to about 10 ppm, so that a rather simple purification loop or, in case of argon, frequent refilling was sufficient.

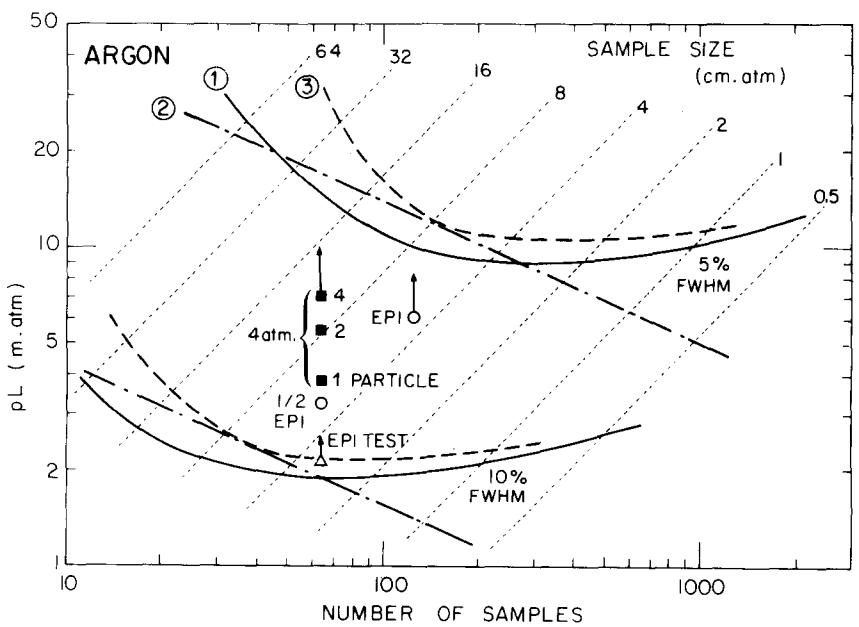

Fig. 17. Comparison of 3 methods of determination of design parameters of dE/dx sampling detectors.

Table 6
Results of joining subsequent tracks (see text for details).

Pressure (atm)	(40%) Fwhm (%)		
	64×4 cm	128×4 cm	256×4 cm
1	12.2	10.0	8.0
	(9.0)	(6.5)	(4.8)
4	7.9	6.1	4.9
	(5.6)	(4.2)	(3.2)

Use of xenon at atmospheric pressure could replace argon at about 3 atm if the price of the order of 10 Frs per liter of xenon for large quantities is economically acceptable. The relativistic rise is higher than in argon, but there are some indications that the resolution per sample will be only slightly improved as compared to argon. This should be verified very carefully, together with studies of gas purity requirements. Another problem is scattering in xenon, which has a radiation length about 8× shorter than argon (this is preventing any reliable resolution studies using radioactive β^- sources). For operation in magnetic fields xenon is better than argon, the Lorenz angle being smaller.

Another possibility for limited total depth applications will be to replace the required increase in pressure of argon by an increase of density of gas due to lower temperatures, so avoiding the pressure vessel and related mechanical and other problems. Operation at temperatures near 100 K is probably possible, especially if the cooling plant for a superconducting solenoid surrounding the detector could be used and if the water condensation problems could be fully solved.

The following suggestions could be made concerning the dE/dx sampling in a colliding beam detector (more information concerning other aspects of the experimental arrangements can be found in refs. 18 , 19):

a) Because of a direct conflict between requirements for high gas amplification factor of typically about 5×10^4 or more for track reconstruction by drift time measurements (especially if charge-division method is used to determine the coordinate along the wires), and typically about 5×10^3 max. imposed by limits of linearity of charge response, it will be preferable to separate the coordinate and amplitude measurements. A compromise in choice of gas mixture and operating conditions is possible. (The conflicting demands are due to different E/p values and drift velocity saturation.)

b) In connection with previously mentioned separation of functions it might be considered worthwhile to make one more step and define the individual samples at 1×1 to $2 \times 2\,cm^2$ level by field wires and abandon the drift. The two-track resolution obtained by fast multi-hit electronics in relatively large drift space will be practically of the same order. In the suggested solution the electronics could be much slower (reduced loss of signal by shaping), simpler and therefore cheaper, with single hit capacity. An interaction trigger could be used as a "common" start signal for the data acquisition for which there will for instance be about 20 μs time interval available before the next bunch crossing in the LEP machine. The granularity of the detector will still be adequate, and even the "coarse" hits from the dE/dx sampling will help in the track reconstruction.

c) From several possible geometries of the detector, some variant of the solution used in the CLEO detector [15] seems to be most favourable for dE/dx sampling, if the amount of matter at the boundaries between adjacent sectors could be kept at minimum. This solution offers a modular construction which may be of interest in experimental areas with difficult access. The wires are much shorter compared to the geometry using wires parallel to the beam axis. To avoid excessive numbers of electronics channels, several wires could be suitably grouped without considerable loss in granularity.

d) A choice of the best suitable gas mixture and operating pressure should be made by optimizing for the required maximum momentum. The safety aspects should be taken into consideration; explosive gas mixtures at high pressure in confined space are best avoided. Of course, a gas having minimum diffusion is not always a safe one.

In general, there are still some open problems to be studied in detail, e.g. the exact definition of energy deposit per sample for strongly curved tracks, the influence of build-up of space charge from positive ions in conditions similar to the realistic background conditions and bunch crossing rate, etc.

The design and construction of the pressure vessel is due to G. Linser and G. Schmidlin, to whom we wish to extend our appreciation. We acknowledge the contribution of J.D. Capt in the design and assembly of the detector and we are indebted to the members of the Beam and Detector Group of the EF Division for their participation in the construction work and during the beam tests. Our thanks also go to E. Chiaveri for tuning and operation of the S3 beam. Continuous support and encouragement from Drs. P. Lazeyras and A. Minten were greatly appreciated.

References

[1] I. Lehraus et al., Phys. Scripta 23 (1981) 727.
[2] M. Aderholz et al., Nucl. Instr. and Meth. 118 (1974) 419.
[3] W.W.M. Allison, Phys. Scripta 23 (1981) 348.
[4] A.H. Walenta, Phys. Scripta 23 (1981) 354.

[5] I. Lehraus et al., Nucl. Instr. and Meth. 153 (1978) 347; P. Lazeyras et al., IEEE Trans. Nucl. Sci. NS-26, (1979) 89.
[6] M. Aderholz et al., Nucl. Instr. and Meth. 123 (1975) 237.
[7] I. Lehraus, CERN/EF/BEAM 76-3 (1976).
[8] G. Schultz et al., Rev. Phys. Appl. 12 (1977) 67; F. Sauli, Yellow Report CERN 77-09 (1977); G. Schultz and J. Gresser, Nucl. Instr. and Meth. 151 (1978) 413; H. Daum et al., Nucl. Instr. and Meth. 152 (1978) 541; F. Sauli , Nucl. Instr. and Meth. 156 (1978) 147; P. Warming, DESY-F22-78/01 (1978); U. Gastaldi et al., Nucl. Istr. and Meth. 156 (1978) 257; B. Kröger and M. Werner, Nucl. Instr. and Meth. 156 (1978) 293; B. Jean-Marie et al., Nucl. Instr. and Meth. 159 (1979) 213; L.G. Christoporou et al., Nucl. Instr. and Meth. 163 (1979) 141; Y. Chatelus et al., Nucl. Instr. and Meth. 171 (1980) 127.
[9] D. Fancher et al., Nucl. Instr. and Meth. 161 (1979) 383.
[10] A.H. Walenta et al., Nucl. Instr. and Meth. 161 (1979) 45.
[11] F. Lapique and F. Piuz, Nucl. Instr. and Meth. 175 (1980) 297.
[12] B.F. Wadsworth et al., IEEE Trans. Nucl. Sci. NS-26 (1979) 120.
[13] W.W.M. Allison et al., Nucl. Instr. and Meth. 163 (1979) 331.
[14] W. Farr et al., Nucl. Instr. and Meth. 156 (1978) 283.
[15] R. Ehrlich et al., IEEE Trans. Nucl. Sci. NS-28 (1981) 421, Phys. Scripta 23 (1981) 736.
[16] I. Lehraus and D. Jeanne, Nucl. Instr. and Meth. 93 (1971) 257.
[17] H. Frehse et al., Nucl. Instr. and Meth. 156 (1978) 87; B. Kröger and M. Werner, Nucl. Instr. and Meth. 156 (1978) 293; D. Friedrich et al., Nucl. Instr. and Meth. 158 (1979) 81.
[18] A. Wagner, Phys. Scripta 23 (1981) 446.
[19] K. Winter, Phys. Scripta 23 (1981) 569.
[20] D. Jeanne et al., Nucl. Instr. and Meth. 111 (1973) 287.